

Mauricio Knak de Almeida
MSc Student
University of Santa Cruz do Sul
Postgraduate Programme in Environmental
Technology
Brasil

Ênio Leandro Machado
Professor
University of Santa Cruz do Sul
Department of Chemistry and Physics
Brasil

Diosnel Antonio R. Lopez
Professor
University of Santa Cruz do Sul
Department of Engineering, Architecture
and Agricultural Science
Brasil

Pâmela Andréa M. dos Santos
Post-Doc Researcher
University of Santa Cruz do Sul
Postgraduate Program in Environmental
Technology
Brasil

Carlos Pérez Bergmann
Professor
Federal University of Rio Grande do Sul
Department of Materials Engineering
Brasil

Adriane de Assis L. Rodriguez
Professor
University of Santa Cruz do Sul
Department of Engineering, Architecture
and Agricultural Science
Brasil

Synthesis of TiO₂-based Photocatalysts and their Use in the Degradation of the Semi-precious-gemstone-coloring Dye Rhodamine B

In this study, new synthetic pathways for the synthesis of TiO₂ were evaluated, and their application in photocatalysis was tested using rhodamine B as a probe. Thermoanalytical analysis (DTA), thermogravimetric analysis (TGA), X-Ray diffraction (XRD), BET method, and scanning electron microscopy (SEM) were employed to characterize the synthesized products. The studied variables included the catalyst type (sol-gel, Pechini, electrospinning and commercial Degussa P-25), the catalyst concentration (0.5 g/L and 2 g/L), the rhodamine B concentration (5 mg/L and 10 mg/L), and the UV irradiation power (32 W and 48 W). A 200 mL reactor was used, and the parameters used to test the treatment efficiency were absorbance and ecotoxicity assays for both the untreated and treated solutions. For rhodamine B degradation, both P-25 and sol-gel TiO₂ presented better photocatalytic efficiency. Ecotoxicity assays showed that the untreated solution had a highly toxic value of EC₅₀ at 48 h (%) for *Daphnia magna*, whereas the solutions treated with either P-25 or sol-gel TiO₂ exhibited no toxicity.

Keywords: Rhodamine B, heterogeneous photocatalysis, titanium dioxide

1. INTRODUCTION

According to the Brazilian Institute for Precious Gems and Metals, Brazil is internationally renowned for the abundance and diversity of precious stones in its soil. The state of Rio Grande do Sul is one of the largest producers of precious stones at the national level and is one of the largest producers of agate and amethyst worldwide [1].

Agate is characterized by its variety of colors, which are displayed as a succession of either straight or concentric parallel bands. The most common colors include gray, blue-gray, white, black, yellow, orange, beige, red, and brown. For the least attractive colors (e.g., gray), one can take advantage of the natural porosity of the mineral and dye them in a different, more desirable, color. This dyeing process can account for up to 40% of the total agate production [2]. Dyeing the gem in does not detract from its commercial value.

Dyeing is the most polluting stage of gem polishing because it can alter several of the following properties: color (turbidity), natural pH, conductivity, chemical and biochemical oxygen demand (COD and BOD,

respectively), and solubilized nutrients (e.g., nitrogen and phosphorus); it can also contaminate or pollute water effluents with heavy metals [3].

The agate production industry, mainly during the dyeing phase, has a high demand for water in its processes, thus generating a high volume of contaminated residual water that contains complex dye molecules. The dye molecules usually employed for this family of gems can be divided into two classes: inorganic or organic. Inorganic dyes are usually composed of acids, such as chromic or nitric acid, combined with other components. The organic dyes frequently contain crystal violet, rhodamine B, and brilliant green. Rhodamine B, for example, is used to imbue a pink coloration to the dyed gems [3,4].

A gradual increase in environmental pollution by industrial effluents over the past several decades has been observed. This pollution represents a serious social and environmental concern. These effluents usually contain toxic and biologically refractory pollutants that cannot be eliminated via the standard techniques (such as coagulation/flocculation, activated charcoal adsorption, precipitation, and biological breakdown) [5].

Technological advances in materials science will certainly focus on a deeper understanding of nanostructured materials [6]. Such materials are known to exhibit physical and chemical properties that significantly differ from those exhibited by the same materials in bulk form. The effects associated with

Received: October 2017, Accepted: December 2017
Correspondence to: Dr Adriane de A. L. Rodriguez
Postgraduate Program of Environmental Technology,
Santa Cruz do Sul-RS, Brasil,
E-mail: adriane@unisc.br
doi:10.5937/fmet1802259K

© Faculty of Mechanical Engineering, Belgrade. All rights reserved

nanometric size are interesting on their own and may serve as a gateway for new applications as well as a means of perfecting currently available technologies.

Therefore, nanomaterials can be regarded as true quantum physics laboratories and a promising source for the development of innovative solutions in innumerable fields and applications [7] as magnetic devices [8], dielectric multiphase composites [9,10], bioengineering materials, pharmaceutical compounds, structural reinforces [11], and solar cells and catalysis, among others.

Porous materials have attracted special attention on their development and applications due mainly to the differentiated mechanical property being able to be used in engineering structures such as ceramics, porous shape memory alloys [8] and foam-like structures [12]. In this way, porous nanostructured or nanoporous materials have been given increasing importance in the fields of molecular separation, catalysis, and gas sensing because of their large surface area, high porosity, and uniform pore size distribution [13].

This study aims to evaluate the use of TiO₂ as photocatalyst for the degradation of the model molecule rhodamine B. In this context, different synthetic pathways for the production of TiO₂ nanodust will be characterized with regard to its possible future application in effluent water treatment. Its efficiency in a photocatalytic reactor with UV irradiation in the breakdown of rhodamine B will also be addressed.

2. MATERIALS AND METHODS

2.1 Synthesis methods for TiO₂ powders

Samples of TiO₂ were synthesized based on the procedure described by [14] using three different pathways—the sol-gel method, the Pechini method and the Electrosynthetic method - using titanium (IV) isopropoxide as a precursor agent.

- **Pechini method synthesis:** Titanium (IV) isopropoxide (108 g) was added to 216 g of citric acid. The mixture was heated to 70 °C under agitation for 30 min, after which 150 mL of distilled water was added. The mixture, still under agitation, was heated to 120 °C, and then, 144 g of ethylene glycol was added. The mixture was left to react under these conditions for 1 h. After a thermal treatment was applied.
- **Sol-gel method synthesis:** One hundred and twenty grams of titanium (IV) isopropoxide was added to 320 g of isopropanol. The mixture, under agitation, was heated at 110 °C for 30 min, and 50 mL of distilled water was then gradually added. The mixture was kept at 110 °C under agitation for 4 h. The mixture was subsequently oven dried at 110 °C, and the a thermal treatment was applied.
- **Electrosynthetic synthesis:** For this method, an experimental setup was built with a voltage controller, a plastic syringe, a capillary-tube kit, a grounded collector and a flow controller. The syringe was pre-filled with solution, and its flow was controlled using

an injection pump. The pump was connected via capillary tubing to the voltage controller, the ground cable was connected to the collector. The collector was turned on, and the voltage difference was measured while the solution flowed through the system. Fiber deposition in the collector usually started when the jet emission voltage was matched. Fibers were collected over the following 30 min.

2.2 Thermal treatment of TiO₂ powders

The obtained samples were placed into a muffle furnace to remove all traces of organic matter and solvent residues according to the procedure described by [14]. The samples were gradually heated in 2.5 °C/min until reach a final temperature of 400 °C , where they remained for 3 h. All samples were subsequently ground with a porcelain mortar and pestle, gradually re-heated in 2.5 °C/min until a final temperature of 600 °C was reached, and maintained for 3 h.

The sample obtained by Electrosynthetic [15] was submitted to a different thermal treatment in a muffle furnace. The treatment consisted of a gradual temperature increase in 1.4 °C/min until reach a final temperature of 700 °C , which was maintained for 3 h.

2.3 Characterization of the synthesized TiO₂

The crystallinity of the synthesized TiO₂ samples was determined by X-Ray Diffraction (XRD) using a Philips X'Pert diffractometer equipped with a Cu K α radiation source ($\lambda = 1.5418 \text{ \AA}$).

Thermogravimetric analysis (TGA) and Thermoanalytical differential analysis (DTA) of the synthesized TiO₂ was performed on a Mettler Toledo TGA/SDTA 851e and on a thermobalance Harrop ST-736, respectively. These tests are largely adopted in various cases for investigating the material status and process phenomena [17, 18]. In both analysis the samples were analyzed in the temperature range of 30 to 1000 °C using a ramp rate of 10 °C·min⁻¹ under a flow of compressed air (10 mL/h). Alumina was used as a control standard. All samples used in these characterizations had been previously dried in a muffle furnace at a temperature of 100 °C for 12 h.

The morphology of the synthesized TiO₂ was assessed using Scanning Electron Microscopy (SEM) on a Vega Plus TS 5136 MM, a TeScan, and a JEOL JSM 6060 setup for this task. A JEOL 6300 Field-Emission Scanning Electron Microscope (FE-SEM) was used for of high-resolution images.

The surface area, pore volume and pore diameter were determined using BET and BJH theories respectively, with help of an Autosorb Quantachrome Instrument Nova 1000 device. Five N₂ adsorption points were collected at a temperature of -196 °C (liquid nitrogen). All samples were vacuum-dried at a temperature of 70 °C for 3 h before analysis.

2.4 Photocatalysis

The different titanium powders synthesized using the different previously discussed methodologies were

analyzed on the photocatalytic reactor. For this purpose, a batch reactor was built that consisted of a 200 mL beaker that contained distilled water with two different rhodamine B (RB) dye concentrations (5 mg/L and 10 mg/L). The photocatalytic efficiency of the nanostructured powders was carried out on a magnetic stirring plate irradiated by UV lamps, which emitted radiation at a range of wavelengths of 350-400 nm. Two different power levels lamps were tested: 32 and 48 W.

The final concentrations of the water-suspended photocatalysts were 0,5 g/L and 2,0 g/L. Samples were collected at time intervals of 0, 2, 4, and 8 h and were then set in a spectrophotometer to analyze the loss of color and, later, the breakdown of its compounds by ecotoxicity assays.

Ecotoxicity assays were performed by exposure of *Daphnia magna* to different concentrations of the sample for 48 h. Based on the immobility of the tested organisms, a total percentage of dead cells per unit concentration was calculated and the EC₅₀ 48 h was estimated according to the probit statistics method for parametric data and the trimmed Spearman-Karber method for non-parametric data [19].

3. RESULTS AND DISCUSSION

3.1 Characterization of the materials

After the thermal treatment of the materials, XRD analyzes were performed. The diffractograms obtained from the different TiO₂ production methods show the characteristic peaks for the material, as can be seen in Figures 1, 2, 3 and 4.

When the sol-gel method was used to generate TiO₂, two phases were observed, anatase and rutile, which were present in a 3:1 ratio. The Pechini method yielded 100% anatase. This variation in the anatase: rutile ratios can lead to different photocatalytic properties [17].

In both thermodifferential and thermogravimetric analyses (Figures 5 and 6), the resulting curves reflect two different stages of thermal decomposition, as expected. An endothermic event up to 100 °C was observed, which was attributed to a loss of water from the material. Then, a peak at 400 °C was observed, which reflected an exothermic area because of the combustion of organic matter. At temperatures greater than 400 °C, the oxide starts to form, and crystal rearrangements occur.

In Figure 7, micrographs of the different TiO₂ materials obtained using SEM are shown at a 1000-fold magnification. The images reveal significantly different morphologies between the materials prepared using different synthetic pathways. Both the sol-gel and electrospinning methods produced well-defined, regularly sized particles with nanometric dimensions, whereas the Pechini method yielded micrometer-scale particles. These results thus link particle size with photocatalytic efficiency.

The SEM images of the electrospinning-derived fibers revealed a uniform shape, with a fiber length that varied from 10 to 100 µm and a diameter of less than 1 µm, in accordance with other similar studies available in the literature. The Pechini method, conversely, may originate clustering of the mineral, with a heterogeneous distribu-

tion. SEM images of the samples obtained via sol-gel synthesis show clustered spherical particles with an average diameter of less than 1 µm, thus originating nanometer-scale particles. The same size of particles was observed in products prepared using the Degussa P-25 method.

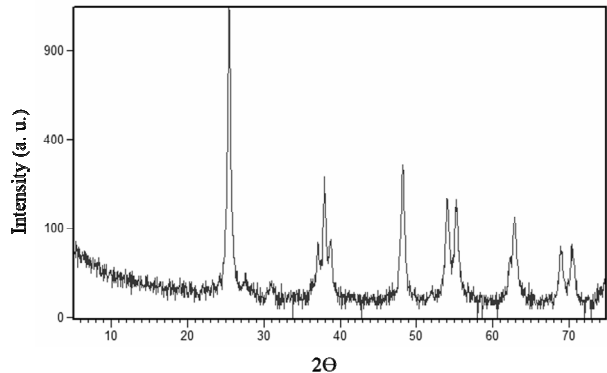


Figure 1. XRD patterns of TiO₂ obtained for sol-gel method.

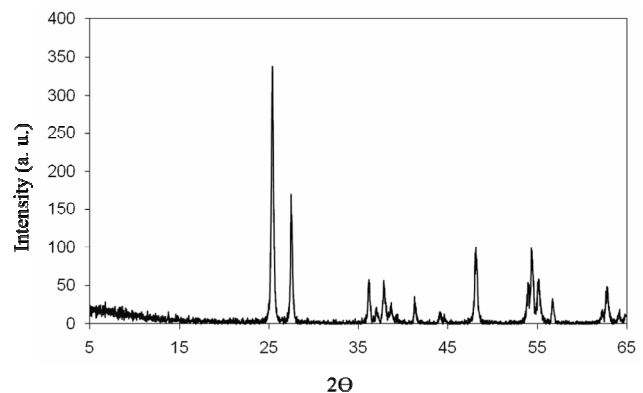


Figure 2. XRD patterns of TiO₂ obtained for Electrospinning method.

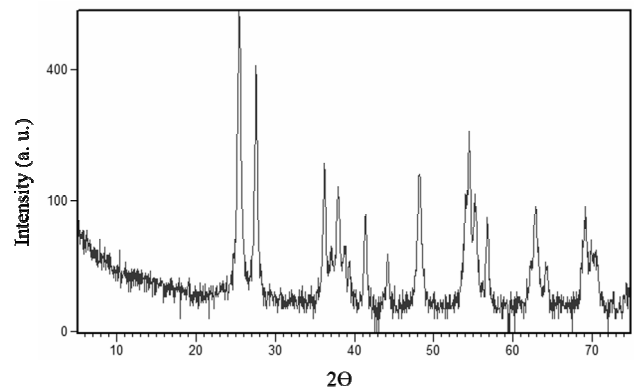


Figure 3. XRD patterns of TiO₂ obtained for Pechini method.

Table 1 shows the values for specific surface area, particle volume and pore size calculated from the BET and BJH analysis.

Table 1. Surface area, pore size and pore volume determined using the BET and BJH method.

Method	Specific surface area (m ² /g)	Total pore volume (cc/g)	Average pore size (nm)
Electro-spinning	51,67	0,09	2,57
Pechini	17,43	0,04	4,74
Sol-gel	26,01	0,08	6,30
P-25	57,19	0,11	3,49

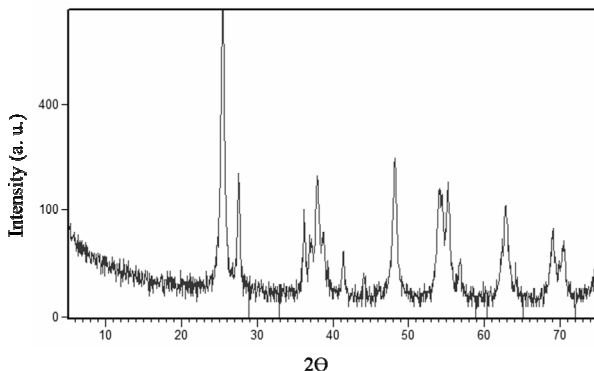


Figure 4. XRD patterns of TiO_2 obtained for P-25.

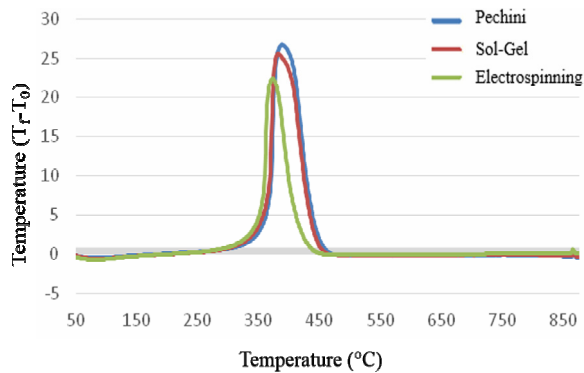


Figure 5. Thermodifferential analysis of nanostructured material.

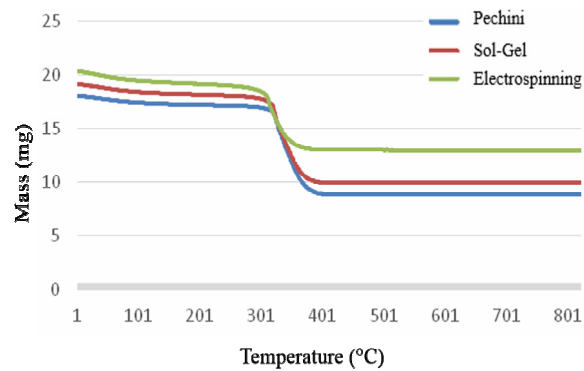


Figure 6. Thermogravimetric analysis of nanostructured material.

The P-25 exhibited the largest surface area ($\sim 57 \text{ m}^2/\text{g}$), followed by the electrospinning fibers ($\sim 51 \text{ m}^2/\text{g}$) and the relatively smaller sol-gel particles ($\sim 26 \text{ m}^2/\text{g}$ and $\sim 17 \text{ m}^2/\text{g}$). Sol-gel particles exhibited the largest average pore size.

Figure 7 show SEM images of TiO_2 . It is possible to see the different morphologies for TiO_2 materials according to the synthesis.

3.2 Photocatalytic activity

The results of the photocatalytic efficiency assays are summarized in Tables 2 and 3.

The sol-gel nanodust is remarkably effective in suspension, even when compared with the commercially available Degussa P-25 TiO_2 . Its net efficiency was superior when compared to the electrospinning and the particles prepared using the Pechini method. The latter method resulted in the least-efficient particles.

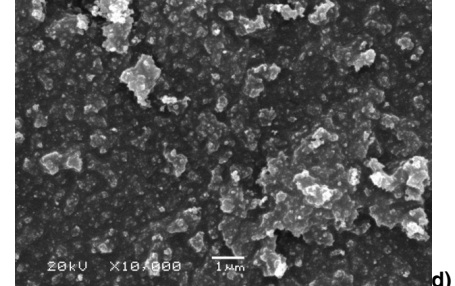
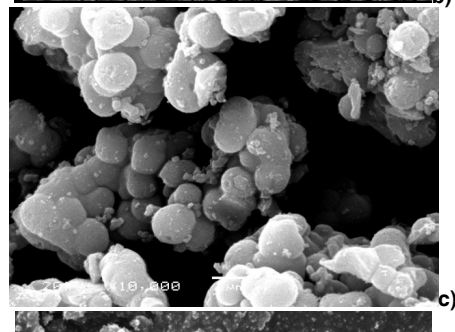
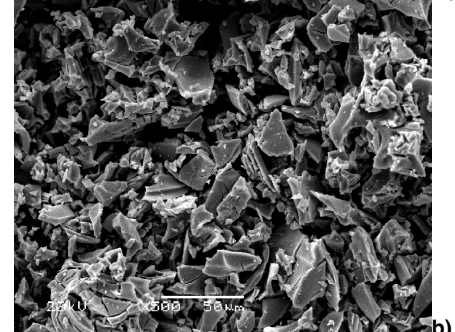
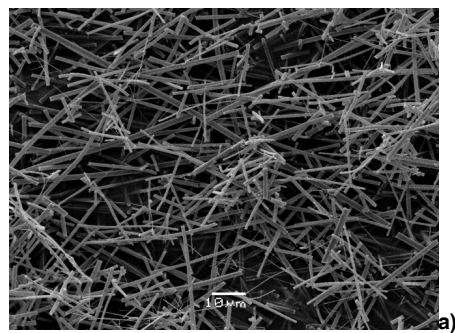


Figure 7. SEM images of TiO_2 materials prepared by: (a) Electrospinning, (b) Pechini, (c) Sol-gel and (d) P-25 Degussa.

Given the previously discussed results, we highlight the following P-25 and sol-gel reaction conditions in terms of efficiency:

- TiO_2 concentration = 2 g/L; power = 48 W; rhodamine B concentration = 5 mg/L; the P-25 material was 92,92% efficient, whereas the sol-gel material yielded 96,94% efficiency.

- TiO_2 concentration = 2 g/L; power = 48 W; rhodamine B concentration = 10 mg/L; the P-25 material was 80,05% efficient, whereas the sol-gel material yielded 95,04% efficiency.

In the Table 4 it is possible to see the kinetics constant for all samples. Samples n°. 1, 7, 11, 12, 17, 36 and 37 represented for P-25 and sol-gel, presented better kinetics constant for degradation of rhodamine B. Figure 8 shows the graphic with these results for the experimental conditions performed.

Table 2. Photocatalytic efficiency (TiO_2 concentration = 0.5 g/L).

	Photocatalytic Efficiency (%)				
	P-25	Sol-gel	Pechini	Electro-spinning	Only UV
5 mg/L of RB 32 W	80.91	71.06	7.77	23.54	0
10 mg/L of RB 32 W	39.29	39.79	14.87	31.02	0
5 mg/L of RB 48 W	86.40	88.72	12.81	35.42	0
10 mg/L of RB 48 W	41.98	43.46	7.05	3.07	0

Table 3. Photocatalytic efficiency (TiO_2 concentration = 2.0 g/L).

	Photocatalytic Efficiency (%)				
	P-25	Sol-gel	Pechini	Electro-spinning	Only UV
5 mg/L of RB 32 W	85.74	91.05	16.50	39.65	0
10 mg/L of RB 32 W	50.07	63.26	10.88	6.71	0
5 mg/L of RB 48 W	92.92	96.94	11.96	45.78	0
10 mg/L of RB 48 W	80.05	95.04	28.13	21.08	0

Table 4. Kinetics constant (k) for each situation.

Sample n°.	Powder	Rhodamine B Concentration (mg/L)	Catalyst Concentration (g/L)	Radiation (W)	$k (\text{min}^{-1})$	R^2
1	P-25	5	0,5	32	$3,3 \times 10^{-3}$	0.9247
2	Sol-gel	5	0,5	32	$2,6 \times 10^{-3}$	0.9718
3	Pechini	5	0,5	32	$6,0 \times 10^{-4}$	0.9749
4	Fibra	5	0,5	32	$2,0 \times 10^{-4}$	0.9578
5	Only UV	5	0,5	32	$6,0 \times 10^{-5}$	0.7511
6	P-25	5	2	32	$2,6 \times 10^{-3}$	0.9579
7	Sol-gel	5	2	32	$3,9 \times 10^{-3}$	0.9073
8	Pechini	5	2	32	$1,8 \times 10^{-3}$	0.9863
9	Fibra	5	2	32	$1,3 \times 10^{-3}$	0.9962
10	Only UV	5	2	32	$4,0 \times 10^{-5}$	0.1531
11	P-25	5	0,5	48	$4,4 \times 10^{-3}$	0.9163
12	Sol-gel	5	0,5	48	$4,0 \times 10^{-3}$	0.8992
13	Pechini	5	0,5	48	$9,0 \times 10^{-4}$	0.9970
14	Fibra	5	0,5	48	$3,0 \times 10^{-4}$	0.9593
15	Only UV	5	0,5	48	$2,0 \times 10^{-5}$	0.9031
16	P-25	5	2	48	$1,3 \times 10^{-3}$	0.9845
17	Sol-gel	5	2	48	$6,5 \times 10^{-3}$	0.7732
18	Pechini	5	2	48	$3,0 \times 10^{-4}$	0.9210
19	Fibra	5	2	48	$1,3 \times 10^{-3}$	0.9845
20	Only UV	5	2	48	$5,0 \times 10^{-6}$	0.1575
21	P-25	10	0,5	32	$1,0 \times 10^{-3}$	0.9929
22	Sol-gel	10	0,5	32	$1,0 \times 10^{-3}$	0.9913
23	Pechini	10	0,5	32	$8,0 \times 10^{-4}$	0.9891
24	Fibra	10	0,5	32	$3,0 \times 10^{-4}$	0.8744
25	Only UV	10	0,5	32	$1,0 \times 10^{-5}$	0.9258
26	P-25	10	2	32	$1,4 \times 10^{-3}$	0.8273
27	Sol-gel	10	2	32	$2,1 \times 10^{-3}$	0.9934
28	Pechini	10	2	32	$2,0 \times 10^{-4}$	0.9145
28	Fibra	10	2	32	$1,0 \times 10^{-4}$	0.9568
30	Only UV	10	2	32	$4,0 \times 10^{-6}$	0.1832
31	P-25	10	0,5	48	$1,2 \times 10^{-3}$	0.9658
32	Sol-gel	10	0,5	48	$1,2 \times 10^{-3}$	0.9829
33	Pechini	10	0,5	48	$2,0 \times 10^{-4}$	0.9715
34	Fibra	10	0,5	48	$7,0 \times 10^{-5}$	0.9804
35	Only UV	10	0,5	48	$4,0 \times 10^{-6}$	0.0479
36	P-25	10	2	48	$6,4 \times 10^{-3}$	0.9115
37	Sol-gel	10	2	48	$3,2 \times 10^{-3}$	0.8341
38	Pechini	10	2	48	$7,0 \times 10^{-4}$	0.9370
39	Fibra	10	2	48	$5,0 \times 10^{-4}$	0.9644
40	Only UV	10	2	48	$9,0 \times 10^{-6}$	0.6396

As P-25 and sol-gel presented the major response for degradation, ecotoxicity assays were performed to evaluate the detoxification properties of TiO₂ for these samples. The untreated solution ecotoxicity, according to the EC₅₀ 48 h (%) scale for *Daphnia magna*, was shown to be extremely high. For a concentration of 0.5 g/L of rhodamine B, untreated solution showed high toxicity (47.88%) and treated solution was non-toxic (100%) and for a concentration of 1 g/L of rhodamine B, untreated solution showed high toxicity (42.04%) and treated solution was non-toxic (100%). The rhodamine B solutions treated with either the sol-gel particles or P-25 did not exhibit toxicity according to the assays performed on *Daphnia magna*.

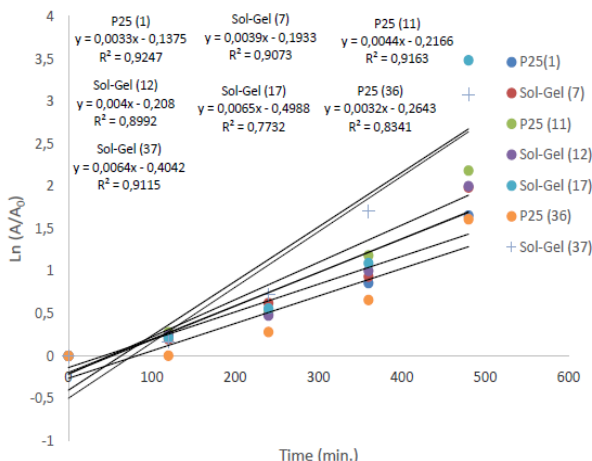


Figure 8. Kinetics curve for degradation of RB for specific experimental conditions.

Figure 9 shows the color difference of the rhodamine B samples with different parameter configurations for decolorization. It is possible to see the influence of each one as well as the behavior of the different TiO₂ powders.

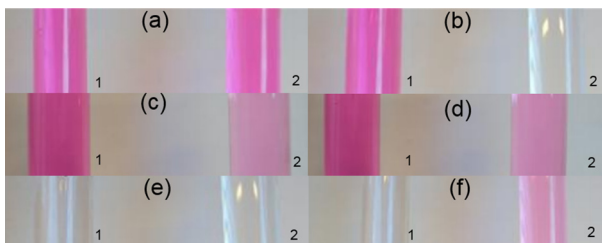


Figure 9. Color difference of rhodamine B samples with different parameter configurations: (a) 1: No treatment, without catalyst, 10mg/L of RB; 2: No treatment, with catalyst, 10mg/L of RB; (b) 1: No treatment, with catalyst, 10mg/L of RB, 2: With treatment, 10mg/L of RB, 2 g/L TiO₂ (sol-gel); (c) 1: No treatment, without catalyst, 10mg/L of RB, 2: With treatment, 10mg/L of RB, 2 g/L TiO₂ (Pechini); (d) 1: No treatment, without catalyst, 10mg/L of RB, 2: With treatment, 10mg/L of RB, 2 g/L TiO₂ (Electrospinning); (e) 1: With treatment, 10mg/L of RB, 2 g/L TiO₂ (Sol-gel), 2: With treatment, 10mg/L of RB, 2 g/L TiO₂ (P-25); (f) 1: With treatment, 10mg/L of RB, 2 g/L TiO₂ (P-25), 2: With treatment, 10mg/L of RB, 2 g/L TiO₂ (Pechini).

4. CONCLUSION

Samples of TiO₂ were prepared via different synthetic pathways, which allowed for a thorough analysis and correlation between the different synthetic pathways and the photocatalytic efficiencies of the samples.

XRD analysis showed that the sol-gel pathway yielded a mixture of anatase and rutile mineral forms

(77% and 23%, respectively). Polymeric precursor synthesis, in turn, yielded 100% of anatase. These two proportions of the mineral forms were considered to be the most efficient in terms of photocatalysis, although during the course of this study, we concluded that the particles prepared using the sol-gel route exhibited a vastly superior performance.

SEM analysis established that the sol-gel, electro-spinning, and P-25 methods yielded morphologically homogeneous, nanometer-sized particles, whereas the Pechini method produced micrometer-sized particles.

Among the tested materials, both the electrospinning and P-25 method had larger surface areas, smaller pore sizes and overall larger pore volumes. Although the sol-gel particles did not exhibit the best characteristics according to the BET method, it was more efficient than the electrospinning method in photocatalysis under the conditions tested.

The following experimental conditions for the sol-gel and P-25 particles yielded the highest efficiencies: a) TiO₂ concentration = 2 g/L; power = 48 W; rhodamine B concentration = 5 mg/L; the P-25 material was 92.92% efficient, whereas the sol-gel material yielded 96.94%. b) TiO₂ concentration = 2 g/L; power = 48 W; rhodamine B concentration = 10 mg/L; the P-25 material was 80.05% efficient, whereas the sol-gel material yielded 95.04%.

The ecotoxicity assays relative to *Daphnia magna* EC₅₀ 48 h (%) varied from highly toxic for the untreated solution to non-toxic for the treated solution.

Heterogeneous photocatalysis using TiO₂ particles was shown to be a good alternative in the treatment of non-biodegradable pollutants, at least when applied to test molecule rhodamine B, due to the inability of conventional methods for treatment of effluents with recalcitrant characteristics.

ACKNOWLEDGMENT

The authors would like to thank CNPq and CAPES for the financial support.

REFERENCES

- [1] Instituto Brasileiro de Gemas e Metais Preciosos, *Annual Report*, 2017.
- [2] Branco, P. M.: *Gemas tratadas*, Serviço Geológico do Brasil, Brazil, 2017.
- [3] Senger, A.M.A.: *Tratamento de esfente das indústrias de beneficiamento de pedras preciosas*. Universidade Federal do Rio Grande do Sul, Porto Alegre, 2005.
- [4] Machado, E.L., et al.: Use of ozonation for the treatment of dye wastewaters containing Rhodamine B in the agate industry, *Water, Air, & Soil Pollution*, Vol. 223, No. 4, pp. 1753-1764, 2012.
- [5] Salgado, B.C.B. et al.: Decolorization of synthetic and laundry wastewater containing indigo and azo dyes by the Fenton, photolytic and UV/H₂O₂ processes, *Engenharia Sanitária e Ambiental*, Vol. 14, No. 1, pp. 1-8, 2009.
- [6] Beaumont P.W.R., Soutis C. and Hodzic A. (Editors): *Structural integrity and durability of*

- advanced composites: Innovative modelling methods and intelligent design, Woodhead Publishing - Elsevier, Cambridge, UK, 2015.
- [7] Lue, J.T.: Physical properties of nanomaterials, Encyclopedia of Nanoscience and Nanotechnology, Vol. 10, No. 1, 2007.
- [8] Fotouhi, M., Saghafi, H., Brugo, T., Minak, G., Fragassa, C., Zucchelli, A. and Ahmadi, M.: Effect of PVDF nanofibers on the fracture behavior of composite laminates for high-speed woodworking machines, Proceedings of the Institution of Mechanical Engineers, Part C: Journal of Mechanical Engineering Science. Vol. 231, No. 1, pp. 31-43, 2017.
- [9] Dinulović, M., Rašuo, B.: Dielectric properties modeling of composite materials, FME Transactions, Vol. 37 No 3, pp. 113-118, 2009.
- [10] Dinulović, M., Rašuo, B., Dielectric modeling of multiphase composites, Composite Structures, Vol. 93, Issue 12, pp. 3209-3215, November 2011.
- [11] Fragassa, C., Berardi, L., Balsamini, G.: Magneto-rheological fluid devices: an advanced solution for an active control on the wood manufacturing process, FME Transactions, Vol. 44, No. 4, pp. 333-339, 2016.
- [12] Balać, Igor et al.: Modeling of the matrix porosity influence on the elastic properties of particulate biocomposites, FME Transactions, Vol. 40, No. 2, pp. 81-86, 2012.
- [13] Lu, G.Q. and X.S. Zhao: Nanoporous materials: An overview, 2004.
- [14] Silva Filho, R. B.: *Estudo de Caracterização de Rotas Sintéticas de Dióxido de Titânio*, Inorganic Chemistry Post-Graduation Program, Chemistry Institute, University of São Paulo, São Paulo, 2007.
- [15] Alves, A.K., et al.: Photocatalytic activity of titania fibers obtained by electrospinning, Materials Research Bulletin, Vol. 44, No. 2, pp. 312-317, 2009.
- [16] Giorgini, L., Fragassa, C., Zattini, G., and Pavlovic, A.: Acid aging effects on surfaces of PTFE gaskets investigated by Fourier Transform Infrared Spectroscopy, Tribology in Industry, Vol. 38, No. 3, pp. 286-296, 2016.
- [17] Fragassa, C., Giorgini, L., Pavlovic, A. and Zattini, G: Acid aging effects on surfaces of PTFE gaskets investigated by Thermal Analysis, Tribology in Industry, Vol. 38, No. 4: pp. 435-444, 2016.
- [18] Lobo, E.A., Rathke, F. S., Brentano, D. M.: Ecotoxicologia aplicada: o caso dos produtores de tabaco na bacia hidrográfica do Rio Pardinho, RS, Brasil. ETGES, VE; FERREIRA, MAF A produção do tabaco: impacto no ecossistema e na saúde humana na região de Santa Cruz do Sul/RS. Santa Cruz do Sul: EDINISC, pp. 41-68, 2006.
- [19] Li, G., et al.: Synthesizing mixed-phase TiO₂ nano-composites using a hydrothermal method for photo-oxidation and photoreduction applications, Journal of Catalysis, Vol. 253, No. 1, pp. 105-110, 2008.
-
- СИНТЕЗА ФОТОКАТАЛИЗATORА НА БАЗИ
TiO₂ И ЊИХОВА УПОТРЕБА У
ДЕГРАДАЦИЈИ ПОЛУДРАГОГ КАМЕЊА
ОБОЈЕН RODAMINOM B**
- М.К. де Алмеида, Е. Л. Махадо, Д. А. Р. Лопез,
П. А. М. дос Сантос, К.П. Бергман, А. Л. Родригез**
- У овом изучавању су процењени нови синтетички путеви за синтезу TiO₂, а њихова примена у фотокатализи тестирана је коришћењем rodamina B као сонде. За карактеризацију синтетизованих производа коришћена је термодиференцијална анализа (DTA), термогравиметријска анализа (TGA), рентгенска дифракција (KSRD), BET метода и скенирање електронске микроскопије (SEM). Испитивање променљивих укључују тип катализатора (sol-gel, Pechini, elektrospinning и комерцијални Degussa P-25), концентрацију катализатора (0,5 g/L и 2g/L), концентрација rodamina B (5 mg / L и 10 mg / L) и моћ UV зрачења (32 V i 48 V). Коришћен је 200 mL реактор, а параметри коришћени за испитивање ефикасности су испитивања апсорбације и екотоксичности за не третиране и третирале растворе. За деградацију родамина B, и P-25 и sol-gel TiO₂ су показали велику фотокаталитичку ефикасност. Анализе екотоксичности показале су да необрађени раствор има високо токсичну вредност EC50 у 48h (%) за Daphnia magna, док раствори третирани или P-25 или sol-gel TiO₂ нису показали токсичност.